

CFD Analysis of Flow Through an Over-Expanded Nozzle

Graham Wilson, AER

December 12, 2024

Contents

1.0	Introduction	1
2.0	Governing Equations	1
2.1	Continuity Equation	2
2.2	Momentum Equations	2
2.3	Energy Equation	3
2.4	Equation of State	3
2.5	Turbulence Modelling: Transition SST ($k - \omega$ based)	3
3.0	Numerical Methodology and Solver Settings	4
4.0	Computational Domain and Mesh	5
4.1	Domain Geometry	5
4.2	Meshing Strategy	5
5.0	Fluid Properties and Boundary Conditions	7
5.1	Fluid Properties	7
5.2	Boundary Conditions	8
6.0	Simulation Results and Discussion	9
6.1	Mach Number Distribution	9
6.2	Static Pressure Distribution	11
6.3	Static Temperature Distribution	12
6.4	Total Pressure Distribution	13
6.5	Turbulent Kinetic Energy (TKE) Distribution	14
6.6	Density Distribution	15
6.7	Overall Flow Features and Comparison with Theory	16
7.0	Critique of the Simulation and Potential Improvements	17
7.1	Strengths of the Simulation	17
7.2	Areas for Improvement and Further Investigation	17
8.0	Conclusion	17

Abstract

This report presents a detailed computational fluid dynamics (CFD) analysis of turbulent gas flow through a two-dimensional axisymmetric convergent-divergent nozzle operating under over-expanded conditions. The study utilizes Ansys Fluent, leveraging the Reynolds-Averaged Navier-Stokes (RANS) equations coupled with the Transition SST (Shear Stress Transport) 4-equation turbulence model. The primary objective of this investigation was to explore the complex flow phenomena characteristic of over-expanded nozzles, including shock wave formation, shock-boundary layer interaction, and potential flow separation. The governing equations, methodology, mesh generation strategy, boundary condition specification, and solver settings are outlined. The simulation results, including distributions of Mach number, static pressure, temperature, total pressure, and turbulent kinetic energy, are presented and critically discussed. The analysis focuses on identifying key flow features and comparing them with established theoretical understanding and findings from relevant literature, such as the work by Balabel et al. (2011) on turbulence modeling for rocket nozzles. Finally, a critique of the simulation is provided, discussing the fidelity of the results and suggesting potential areas for improvement, particularly regarding the resolution of shock structures.

1.0 Introduction

Convergent-divergent (CD) nozzles, often referred to as de Laval nozzles, are components in many engineering applications, most notably in rocket propulsion systems, jet engines, and supersonic wind tunnels. Their primary function is to accelerate a fluid to supersonic speeds, thereby maximizing thrust or achieving desired test conditions. The performance of a CD nozzle is highly dependent on the pressure ratio across it, specifically the ratio of the stagnation pressure at the inlet (or chamber pressure) to the ambient or back pressure into which the nozzle exhausts.

A nozzle is said to be operating under "over-expanded" conditions when the static pressure at the nozzle exit (P_e) is lower than the ambient back pressure (P_b). This adverse pressure gradient ($dP/dx > 0$) at the nozzle exit forces the flow to adjust to the higher back pressure, often leading to the formation of complex shock wave patterns within or just outside the nozzle. These shock waves, which can be oblique or normal, interact with the nozzle wall boundary layers, potentially causing flow separation, increased drag, side loads (in asymmetric separation), and reduced overall nozzle efficiency [1, 2].

Understanding the intricate flow physics in over-expanded nozzles is important for accurate performance prediction and robust design. The flow field is characterized by strong pressure gradients, compressibility effects, shock-boundary layer interactions, and significant turbulence production. Accurately predicting these phenomena numerically presents a challenge, with the choice of turbulence model playing a significant role, as highlighted by Balabel et al. [3]. Their work assessed various turbulence models for gas flow in CD rocket nozzles, emphasizing the importance of selecting an appropriate model to capture phenomena like shock position and separation characteristics. The Shear Stress Transport (SST) $k - \omega$ model was found to provide reasonable agreement with experimental data in their study.

This report details a CFD analysis of an over-expanded, two-dimensional axisymmetric CD nozzle. The simulation was performed using Ansys Fluent. This study aims to:

- Numerically predict the turbulent gas flow dynamics within the nozzle.
- Investigate the associated physical phenomena, particularly shock wave structures and their interaction with the flow.
- Evaluate the suitability of the Transition SST turbulence model for this class of flows.
- Provide an understanding of the solver setup, meshing strategy, and boundary conditions employed.
- Analyze and discuss the simulation results, focusing on Mach number, pressure, temperature, and turbulence distributions.
- Offer a critique of the simulation, addressing potential limitations and areas for future refinement.

The insights gained from this analysis contribute to an understanding of over-expanded nozzle flows and the capabilities of modern CFD tools in predicting such complex turbulent, compressible phenomena.

2.0 Governing Equations

The flow of a compressible, turbulent fluid is described by the Reynolds-Averaged Navier-Stokes (RANS) equations, which represent the conservation of mass, momentum, and energy. For the 2D axisymmetric flow considered in this study, these equations can be written in cylindrical coordinates (x for axial, r for radial).

2.1 Continuity Equation

The conservation of mass is given by:

$$\frac{\partial \rho}{\partial t} + \frac{\partial(\rho u_x)}{\partial x} + \frac{1}{r} \frac{\partial(r \rho u_r)}{\partial r} = 0 \quad (1)$$

For the steady-state flow simulation ($\frac{\partial \rho}{\partial t} = 0$):

$$\frac{\partial(\rho u_x)}{\partial x} + \frac{1}{r} \frac{\partial(r \rho u_r)}{\partial r} = 0 \quad (2)$$

where ρ is the density, u_x is the axial velocity component, and u_r is the radial velocity component.

2.2 Momentum Equations

The conservation of momentum, including the Reynolds stress terms for turbulence, is:

Axial Momentum (x -direction):

$$\begin{aligned} \frac{\partial(\rho u_x)}{\partial t} + \frac{\partial(\rho u_x u_x)}{\partial x} + \frac{1}{r} \frac{\partial(r \rho u_x u_r)}{\partial r} &= -\frac{\partial p}{\partial x} \\ &+ \frac{\partial}{\partial x} \left[\mu \left(2 \frac{\partial u_x}{\partial x} - \frac{2}{3} (\nabla \cdot \mathbf{u}) \right) - \rho \overline{u'_x u'_x} \right] \\ &+ \frac{1}{r} \frac{\partial}{\partial r} \left[r \mu \left(\frac{\partial u_x}{\partial r} + \frac{\partial u_r}{\partial x} \right) - r \rho \overline{u'_x u'_r} \right] \end{aligned} \quad (3)$$

Radial Momentum (r -direction):

$$\begin{aligned} \frac{\partial(\rho u_r)}{\partial t} + \frac{\partial(\rho u_r u_x)}{\partial x} + \frac{1}{r} \frac{\partial(r \rho u_r u_r)}{\partial r} &= -\frac{\partial p}{\partial r} \\ &+ \frac{\partial}{\partial x} \left[\mu \left(\frac{\partial u_r}{\partial x} + \frac{\partial u_x}{\partial r} \right) - \rho \overline{u'_r u'_x} \right] \\ &+ \frac{1}{r} \frac{\partial}{\partial r} \left[r \mu \left(2 \frac{\partial u_r}{\partial r} - \frac{2}{3} (\nabla \cdot \mathbf{u}) \right) - r \rho \overline{u'_r u'_r} \right] - \mu \frac{2 u_r}{r^2} + \frac{2}{3} \frac{\mu}{r} (\nabla \cdot \mathbf{u}) + \rho \frac{u_\theta^2}{r} \end{aligned} \quad (4)$$

where p is the static pressure, μ is the dynamic viscosity, and $-\rho \overline{u'_i u'_j}$ are the Reynolds stresses. For the axisymmetric flow without swirl modeled, $u_\theta = 0$. The divergence of velocity is $\nabla \cdot \mathbf{u} = \frac{\partial u_x}{\partial x} + \frac{1}{r} \frac{\partial(r u_r)}{\partial r}$. As the simulation was steady, $\frac{\partial(\cdot)}{\partial t} = 0$.

The Reynolds stresses were modeled using the Boussinesq hypothesis:

$$-\rho \overline{u'_i u'_j} = \mu_t \left(\frac{\partial u_i}{\partial x_j} + \frac{\partial u_j}{\partial x_i} \right) - \frac{2}{3} (\rho k + \mu_t \nabla \cdot \mathbf{u}) \delta_{ij} \quad (5)$$

where μ_t is the turbulent (eddy) viscosity and k is the turbulent kinetic energy.

2.3 Energy Equation

The conservation of energy for a compressible fluid, often expressed in terms of total energy $E = \rho(h + \frac{1}{2}u_i u_i) - p$, where h is static enthalpy, is:

$$\frac{\partial(\rho E)}{\partial t} + \nabla \cdot (\mathbf{u}(\rho E + p)) = \nabla \cdot (k_{eff} \nabla T + (\boldsymbol{\tau}_{eff} \cdot \mathbf{u})) + S_h \quad (6)$$

where $k_{eff} = k_{laminar} + k_{turbulent}$ is the effective thermal conductivity ($k_{turbulent} = \mu_t C_p / Pr_t$), $\boldsymbol{\tau}_{eff}$ is the effective stress tensor (including laminar and turbulent stresses), and S_h represents volumetric heat sources (which were not present in this simulation). For an ideal gas, $h = C_p T$.

2.4 Equation of State

For air, treated as an ideal gas, the equation of state is:

$$p = \rho R T \quad (7)$$

where R is the specific gas constant for air (287.058 J/kg K) and T is the static temperature.

2.5 Turbulence Modelling: Transition SST ($k - \omega$ based)

The Transition SST model was selected, a four-equation turbulence model that builds upon the standard SST $k - \omega$ model by adding two transport equations: one for intermittency (γ) and one for the transition momentum thickness Reynolds number ($\tilde{Re}_{\theta t}$). This selection allowed the model to predict laminar-to-turbulent transition.

SST $k - \omega$ Base Model

The SST $k - \omega$ model [5] combines the robustness of the $k - \omega$ model in the near-wall region with the freestream independence of the $k - \epsilon$ model in the far field.

Turbulent Kinetic Energy (k):

$$\frac{\partial(\rho k)}{\partial t} + \frac{\partial(\rho u_j k)}{\partial x_j} = \tilde{P}_k - \tilde{D}_k + \frac{\partial}{\partial x_j} \left[(\mu + \sigma_k \mu_t) \frac{\partial k}{\partial x_j} \right] \quad (8)$$

Specific Dissipation Rate (ω):

$$\frac{\partial(\rho \omega)}{\partial t} + \frac{\partial(\rho u_j \omega)}{\partial x_j} = P_\omega - D_\omega + D_{\omega,cross} + \frac{\partial}{\partial x_j} \left[(\mu + \sigma_\omega \mu_t) \frac{\partial \omega}{\partial x_j} \right] \quad (9)$$

where \tilde{P}_k is the production of k (modified by intermittency in Transition SST), \tilde{D}_k is the destruction of k (modified by intermittency), P_ω is production of ω , D_ω is destruction of ω , and $D_{\omega,cross}$ is the cross-diffusion term. The turbulent viscosity μ_t is computed as:

$$\mu_t = \frac{\rho k}{\omega} \frac{1}{\max \left[\frac{1}{\alpha^*}, \frac{SF_2}{\alpha_1 \omega} \right]} \quad (10)$$

F_2 is a blending function, S is the magnitude of the strain rate, and α^* is a coefficient that damps turbulent viscosity causing a low-Reynolds number correction. The model constants and blending functions F_1, F_2 are standard for the SST model [5, 6].

Intermittency Transport Equation (γ)

The intermittency equation models the transition from laminar to turbulent flow [7]:

$$\frac{\partial(\rho\gamma)}{\partial t} + \frac{\partial(\rho u_j \gamma)}{\partial x_j} = P_{\gamma_1} - E_{\gamma_1} + P_{\gamma_2} - E_{\gamma_2} + \frac{\partial}{\partial x_j} \left[(\mu + \frac{\mu_t}{\sigma_\gamma}) \frac{\partial \gamma}{\partial x_j} \right] \quad (11)$$

where $P_{\gamma_1}, E_{\gamma_1}$ are production and destruction terms related to local transition onset, and $P_{\gamma_2}, E_{\gamma_2}$ are terms related to destruction/re-laminarization due to flow acceleration or separation. The intermittency γ ranges from 0 (fully laminar) to 1 (fully turbulent). It modifies the production and destruction terms of the k equation.

Transition Momentum Thickness Reynolds Number Transport Equation ($\tilde{Re}_{\theta t}$)

This equation models the transport of a critical Reynolds number based on momentum thickness:

$$\frac{\partial(\rho \tilde{Re}_{\theta t})}{\partial t} + \frac{\partial(\rho u_j \tilde{Re}_{\theta t})}{\partial x_j} = P_{\theta t} + \frac{\partial}{\partial x_j} \left[\sigma_{\theta t} (\mu + \mu_t) \frac{\partial \tilde{Re}_{\theta t}}{\partial x_j} \right] \quad (12)$$

where $P_{\theta t}$ is a source term that depends on local flow conditions and empirical correlations for transition. The full details of the Transition SST model, including all source terms and closure coefficients, are complex and can be found in the works by Menter et al. [6, 7].

3.0 Numerical Methodology and Solver Settings

The simulation was performed using Ansys Fluent, a commercial CFD software package. For the setup, the **Density-Based solver** was selected, which is generally preferred for high-speed compressible flows involving shocks, as it solves the governing equations simultaneously. The velocity formulation was set to **Absolute**. The simulation aimed to find a **Steady-state** solution for the flow field. The nozzle was modeled in **2D Axisymmetric space** to reduce computational cost, assuming symmetrical flow about the nozzle centerline. Gravitational effects were turned **Off**, as they are negligible for high-speed gas flows in nozzles.

For the viscous model, the **Transition SST (4 eqn) model** was chosen. This model is based on the $k - \omega$ Shear Stress Transport (SST) model but includes two additional transport equations for intermittency (γ) and transition momentum thickness Reynolds number ($\tilde{Re}_{\theta t}$). This selection was made to predict potential laminar-to-turbulent transition phenomena, which can be relevant in nozzle boundary layers. The **Energy equation was enabled**, which is essential for compressible flows where temperature variations are significant.

Regarding the solution methods, an **Implicit formulation** was used. The **Flux Type was Roe-FDS** (Roe-Flux Difference Splitting), an upwind scheme well-suited for capturing sharp discontinuities like shock waves. For **Spatial Discretization**, gradients were reconstructed using the **Least Squares Cell Based** method. Flow variables, as well as Turbulent Kinetic Energy, Specific Dissipation Rate, Intermittency, and Momentum Thickness Re, were all discretized using **Second Order Upwind** schemes to balance accuracy

and stability. The Pseudo Time Method was off, relying on Fluent's density-based solver's inherent pseudo-time stepping or non-iterative time-advancement schemes for steady-state solutions.

4.0 Computational Domain and Mesh

4.1 Domain Geometry

The computational domain constructed for this analysis consists of:

1. An inlet section representing the upstream flow straightener or combustion chamber.
2. The convergent-divergent nozzle itself, featuring a converging section, a throat, and a diverging (supersonic) section.
3. An external plenum or exhaust region extending downstream from the nozzle exit plane, allowing the jet to develop and interact with the ambient conditions.

Figure 1 shows a general layout of a typical domain with boundary labels for reference, though the mesh shown in that figure is an example and not the specific one used for the results presented.

Ansys
2022 R2

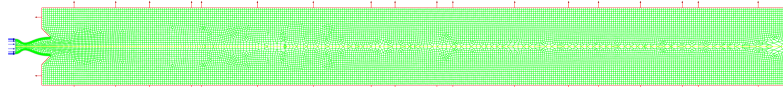


Figure 1: Example mesh showing labeled boundary conditions (for general reference, not the specific mesh used for the results presented).

4.2 Meshing Strategy

An unstructured mesh was generated, composed primarily of triangular elements in the 2D plane, which form prisms or wedges when considered in an axisymmetric context. Figures 2, 3, and 4 illustrate the mesh used.

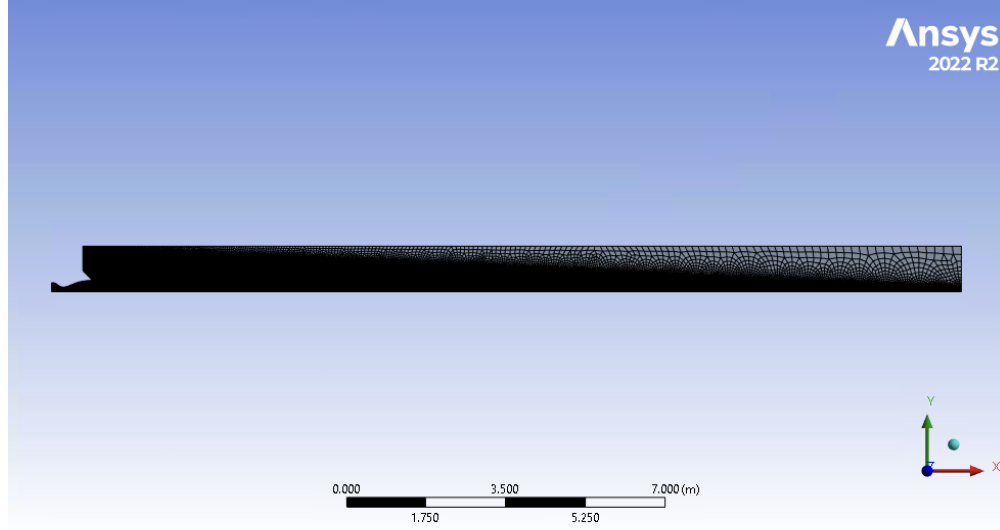


Figure 2: Overall view of the mesh generated for the nozzle and external plenum.

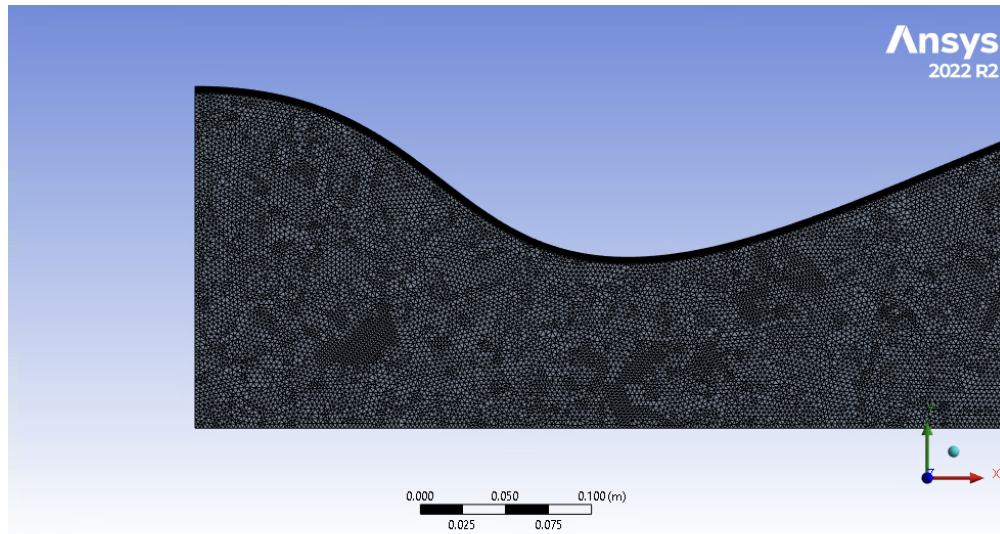


Figure 3: Detailed view of the mesh within the nozzle section.

As shown in Figure 2, the mesh is denser within the nozzle and in the immediate vicinity of the jet plume. Figure 3 provides a closer view of the mesh within the nozzle, where the density appears reasonable for capturing general flow features.

An important aspect of the meshing strategy was boundary layer refinement. Figure 4 shows a structured-like layer of prismatic cells created adjacent to the nozzle wall. This is important for resolving the high velocity and temperature gradients within the boundary layer and for the accurate performance of the Transition SST model, which can benefit from resolving the viscous sublayer ($y^+ \sim 1$). The refinement consists of multiple layers, which is good practice.

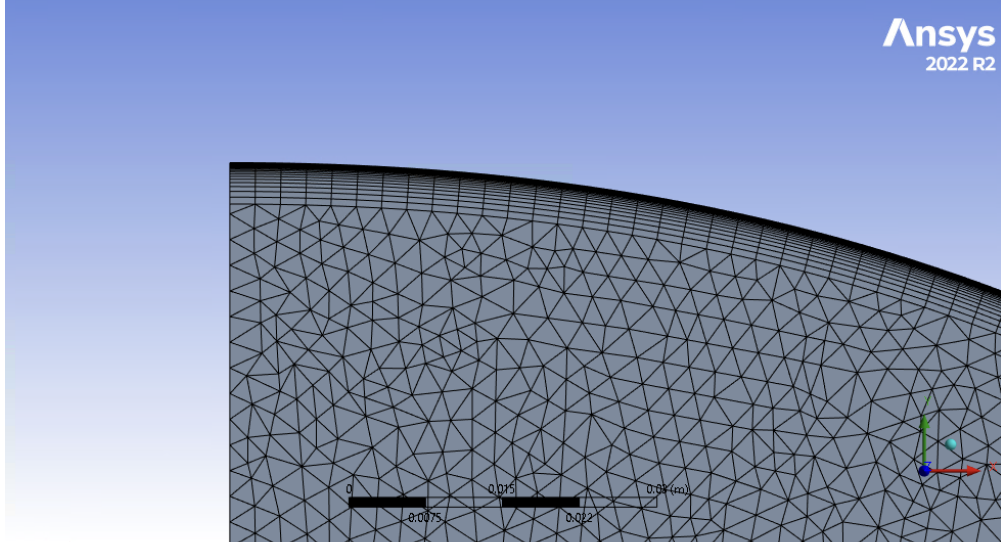


Figure 4: Zoomed-in view of the prismatic inflation layers used near the nozzle wall.

Mesh quality is important for CFD accuracy. Key aspects considered include:

- **Sufficient cell density** in regions of high gradients (throat, shock locations, shear layers).
- **Appropriate near-wall resolution** (y^+ value). While resolving the viscous sublayer ($y^+ \approx 1$) is often recommended for the Transition SST model, it can also work with wall functions if the mesh is coarser. The aim was fine near-wall resolution.
- **Smooth cell size transitions** to avoid numerical errors.
- **Good cell quality** (e.g., low skewness, reasonable aspect ratio).

Without specific mesh statistics (number of cells, y^+ values, skewness) included in this report, a complete quantitative assessment of the mesh quality is difficult, but visual inspection suggested a reasonable attempt at boundary layer refinement and density in regions with high gradients.

5.0 Fluid Properties and Boundary Conditions

5.1 Fluid Properties

The working fluid for the simulation was **air**. Its properties were defined as follows:

- **Density:** Modeled using the Ideal Gas Law ($p = \rho RT$), appropriate for compressible flows with significant density variations.
- **Specific Heat (C_p):** Defined using a NASA 9-piecewise polynomial, allowing for temperature-dependent specific heat, which is more accurate than a constant C_p assumption over a wide range of temperatures.
- **Thermal Conductivity:** Calculated using Kinetic Theory, which typically makes it temperature-dependent.

- **Viscosity:** Also calculated using Kinetic Theory, making it temperature-dependent (e.g., via Sutherland's law or a power law).
- **Molecular Weight:** Constant, 28.966 kg/kmol.
- **L-J Characteristic Length & Energy Parameter:** These parameters for the Lennard-Jones potential (3.711 Angstrom and 78.6 K respectively) were specified, as they are used by some kinetic theory models for transport properties.

5.2 Boundary Conditions

The following boundary conditions were defined to model the interaction of the computational domain with its surroundings:

Inlet (pressure-inlet, id=5)

This boundary was located upstream of the converging section.

- **Type:** Pressure Inlet.
- **Gauge Total Pressure (P_0):** 400000 Pa (gauge). Assuming atmospheric pressure (P_{atm}) is 101325 Pa, the absolute total pressure was $P_{0,abs} = 501325$ Pa.
- **Supersonic/Initial Gauge Pressure ($P_{static,initial}$):** 390000 Pa (gauge). This results in an absolute static pressure $P_{static,initial,abs} = 491325$ Pa, used for initialization and if the inlet flow were to become locally supersonic.
- **Direction Specification Method:** Normal to Boundary.
- **Turbulence Specification Method:** Intermittency, Intensity and Viscosity Ratio.
 - **Intermittency (γ):** 1, implying fully turbulent flow at the inlet.
 - **Turbulent Intensity (%):** 5%, a common value for internal flows when specific data is not available.
 - **Turbulent Viscosity Ratio (μ_t/μ):** 10, further characterizing the incoming turbulence.

Over-Expanded Condition Check (Example): To achieve over-expanded conditions, the nozzle exit pressure (P_e) must be less than the back pressure (P_b). Assuming the outlet exhausts to atmospheric pressure, $P_{b,abs} = 101325$ Pa. Given the inlet total pressure $P_{0,inlet,abs} = 501325$ Pa, the nozzle operates with an overall pressure ratio. If the flow expands within the nozzle such that $P_e < 101325$ Pa, it is over-expanded. The simulation results, discussed later, confirm this condition.

Outlet (pressure-outlet, id=9)

This boundary was at the far end of the external plenum.

- **Type:** Pressure Outlet.
- **Gauge Pressure (P_b):** This was set to 0 Pa (gauge), representing exhaust to standard atmospheric conditions ($P_{b,abs} = 101325$ Pa). This value is important for defining the over-expanded nature of the nozzle.

- Other parameters like backflow temperature and turbulence conditions were set to default or appropriate values.

The contour plots from the simulation confirm that the flow is indeed over-expanded based on this back pressure.

Wall (wall, id=7)

This represented the internal walls of the nozzle and the upstream duct.

- **Type:** Wall.
- **Shear Condition:** No-slip, standard for viscous flows.
- **Thermal Condition:** Adiabatic (zero heat flux). This is a common assumption for nozzle performance studies unless specific wall cooling/heating is being modeled, aligning with Balabel et al. [3] who also assumed adiabatic walls.

Axis (axis, id=6)

This was the centerline of the axisymmetric domain.

- **Type:** Axis.
- Fluent applies symmetry conditions here: zero radial velocity ($u_r = 0$) and zero normal gradients for all other variables ($\partial\phi/\partial r = 0$).

Internal (interior-nozzle_latest, id=1)

This was not a physical boundary but an internal face zone created during meshing, likely separating different mesh regions. Fluent treats these as fully continuous, ensuring no artificial interface effects.

6.0 Simulation Results and Discussion

6.1 Mach Number Distribution

Figures 5 and 6 show the Mach number contours.

- The flow enters subsonically ($M < 1$) and accelerates through the converging section.
- Sonic conditions ($M = 1$) are reached at the throat, as expected for a choked nozzle.
- In the diverging section, the flow accelerates to supersonic speeds ($M > 1$). The maximum Mach number observed inside the nozzle appears to be around $M \approx 2.5 - 2.6$.
- **Over-expansion Shock System:** The results show a complex shock structure within the diverging section, downstream of the throat but before the nozzle exit. This pattern is characteristic of over-expanded nozzle flow. It appears as an oblique shock wave reflecting from the nozzle centerline, forming a "shock diamond" or Mach reflection pattern. This shock system recompresses the flow, causing a sudden decrease in Mach number and an increase in static pressure and temperature.

- The jet exiting the nozzle remains supersonic initially but interacts with the ambient pressure, leading to further shock/expansion wave patterns in the external plume, visible in Figure 6.
- The presence of these shocks inside the diverging part confirms that the nozzle was operating in an over-expanded regime where $P_e < P_b$, and the flow adjusts to P_b via these shocks.

The clarity of the shock waves in the contour plots is somewhat diffuse. This could be due to limitations in mesh resolution or numerical dissipation inherent in the second-order schemes used. Sharper shock capturing typically requires finer meshes in the shock region and/or higher-order discretization schemes with appropriate shock-capturing limiters.

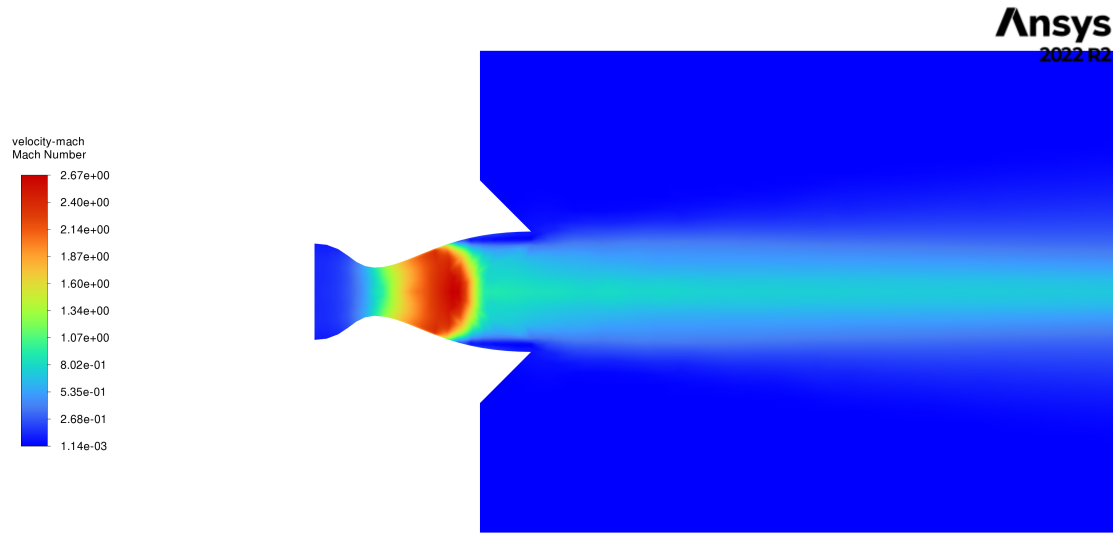


Figure 5: Mach Number contours (nozzle detail).

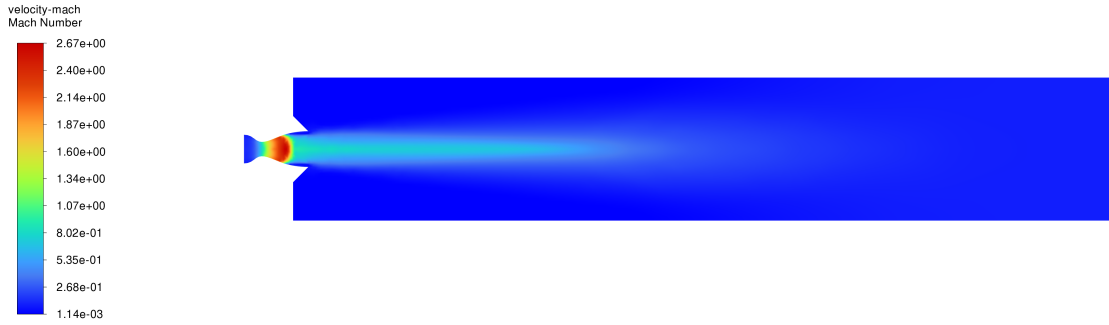


Figure 6: Mach Number contours (full domain).

6.2 Static Pressure Distribution

Figure 7 shows the static pressure contours.

- Static pressure decreases as the flow accelerates through the converging section and the throat.
- In the diverging section, static pressure continues to drop as the flow expands supersonically.
- Across the internal shock waves, there is a sharp increase in static pressure due to flow recompression. The pressure downstream of the shock is higher than the pressure just upstream of it.
- The pressure at the nozzle exit plane (P_e) appears significantly lower than the initial inlet static pressure and, as inferred from the shock system, lower than the ambient back pressure P_b before the shock system begins to adjust it.
- The pressure distribution in the exhaust plume shows further adjustments (waves of compression and expansion) as the jet interacts with the ambient environment.

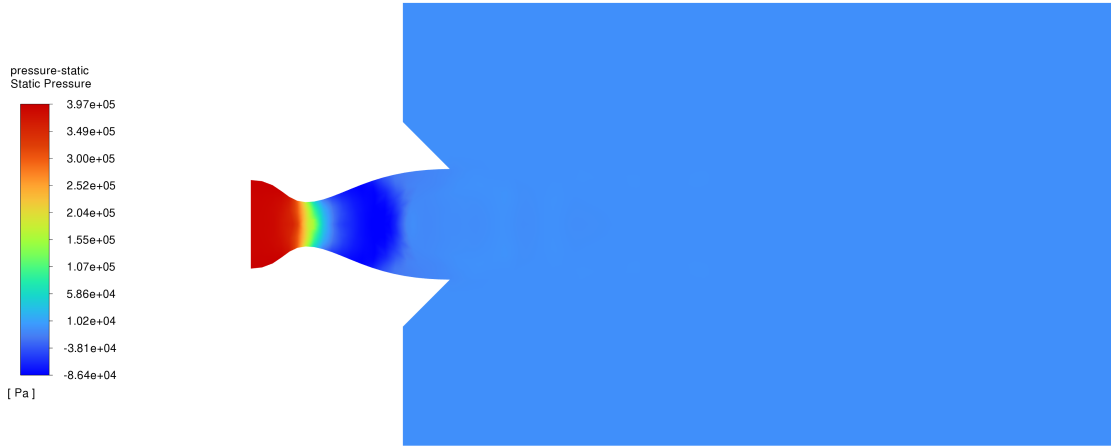
Ansys
2022 R2

Figure 7: Static Pressure contours.

6.3 Static Temperature Distribution

Figure 8 shows the static temperature contours.

- Static temperature decreases as the flow accelerates and expands, converting thermal energy into kinetic energy. This is evident in the converging section, throat, and the initial part of the diverging section.
- Across the shock waves, there is a significant increase in static temperature due to the dissipative nature of shocks and flow recompression.
- The temperature at the core of the jet remains relatively low where the Mach number is high, and increases in regions of lower Mach number or after shock compression.

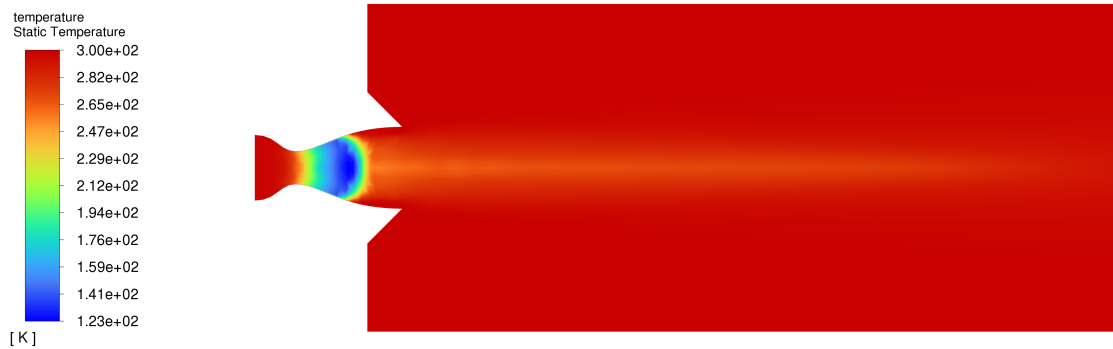


Figure 8: Static Temperature contours.

6.4 Total Pressure Distribution

Figure 9 shows the total pressure contours.

- Total pressure (P_0) remains nearly constant in isentropic flow regions (away from walls and shocks). Some loss is expected in the boundary layers due to viscous effects, which the simulation captures.
- **Across the shock waves, there is a significant and irreversible loss in total pressure.** This is a characteristic of shock waves and represents a major source of inefficiency in over-expanded nozzle operation. The contour plot shows a drop in total pressure downstream of the internal shock system.
- Further total pressure losses occur in the shear layers of the jet plume due to turbulent mixing with the ambient fluid.

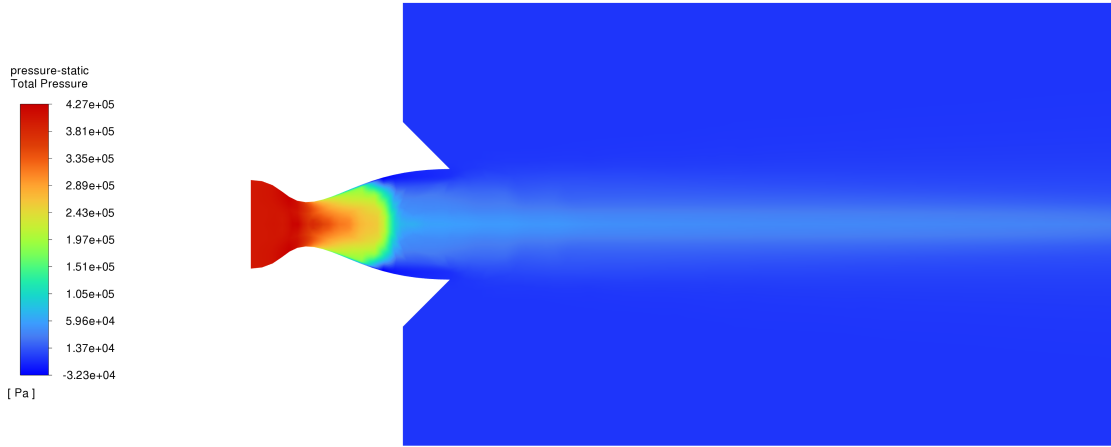
Ansys
2022 R2

Figure 9: Total Pressure contours.

6.5 Turbulent Kinetic Energy (TKE) Distribution

Figures 10 and 11 show the TKE distribution.

- TKE levels are relatively low in the core flow upstream of the shocks.
- Significant TKE production was observed in several regions:
 - **Boundary Layers:** Along the nozzle walls, due to high shear.
 - **Shock-Boundary Layer Interaction (SBLI) Regions:** Where the internal shocks impinge on the nozzle wall boundary layers. SBLI is a strong source of turbulence.
 - **Shear Layers of the Jet:** The interface between the high-speed jet exiting the nozzle and the quiescent ambient fluid is a region of intense shear and, consequently, high TKE production. This is clearly visible in Figure 11.
 - Potentially within the shock structures themselves due to strong velocity gradients and instabilities.
- The Transition SST model used is designed to predict the onset and development of turbulence, and the TKE contours reflect these processes.

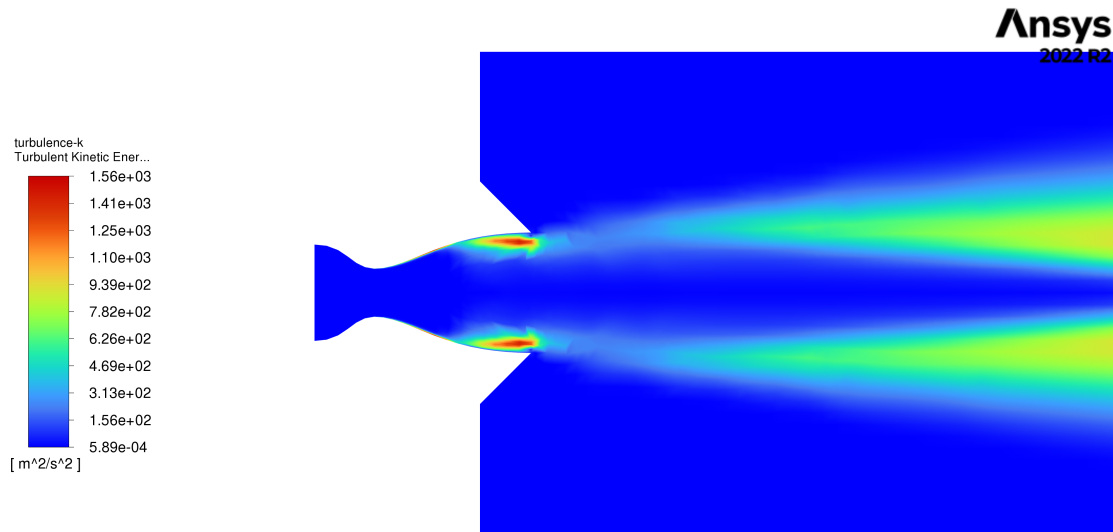


Figure 10: Turbulent Kinetic Energy contours (nozzle detail).

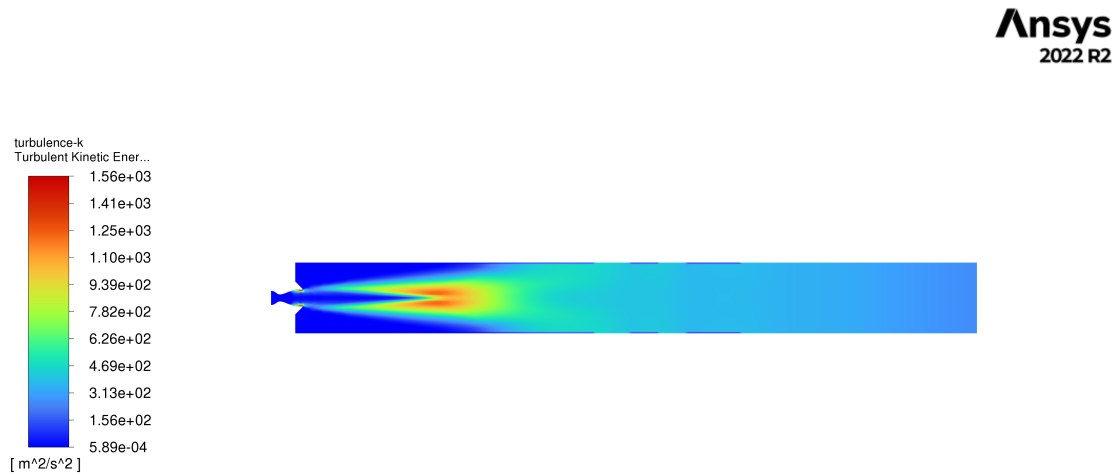


Figure 11: Turbulent Kinetic Energy contours (full domain).

6.6 Density Distribution

Figure 12 shows the density contours.

- Density decreases as the flow expands and accelerates, and increases upon compression through the shock waves.

- The density contours mirror the static pressure and inverse static temperature trends, as expected from the ideal gas law ($\rho = p/(RT)$).

Ansys
2022 R2

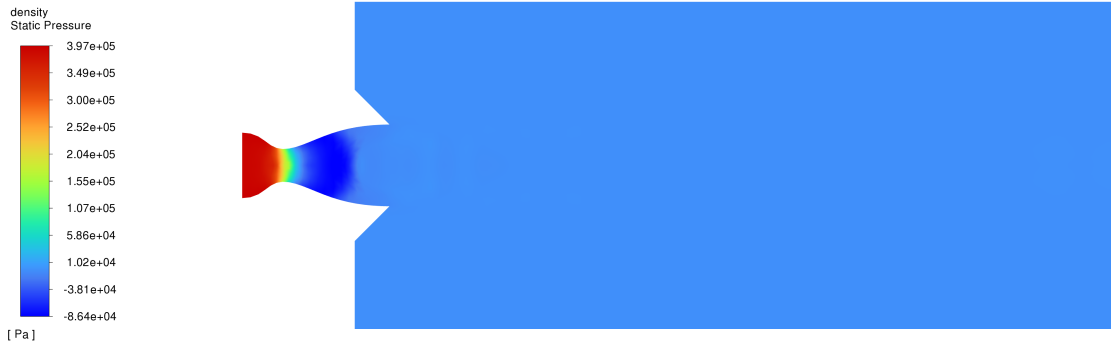


Figure 12: Density contours.

6.7 Overall Flow Features and Comparison with Theory

The simulation successfully captured the key features of over-expanded nozzle flow:

1. Acceleration to supersonic speeds in the diverging section.
2. Formation of an internal shock system (likely oblique shocks and Mach reflections) to adjust the low exit pressure of the supersonic flow to the higher ambient back pressure.
3. Irreversible losses in total pressure across the shocks.
4. Increased static pressure and temperature downstream of the shocks.
5. High turbulence production in shear layers and SBLI regions.

The observed patterns are consistent with theoretical descriptions of over-expanded flows [1, 4]. The work by Balabel et al. [3] also discusses these phenomena, emphasizing that different turbulence models predict varying shock positions and separation characteristics. While a direct comparison to their specific geometry and NPR is not possible without more data, the general phenomena are similar. Their finding that the SST $k - \omega$ model (the basis for Transition SST) performed well for such flows lends confidence to the choice of turbulence model, provided the mesh resolution is adequate.

7.0 Critique of the Simulation and Potential Improvements

7.1 Strengths of the Simulation

- **Appropriate Solver Choice:** The density-based solver used is suitable for this class of high-speed, compressible flow.
- **Advanced Turbulence Model:** The choice of the Transition SST model is sophisticated, capable of handling both turbulent regions and predicting transition, which can be important.
- **Realistic Fluid Properties:** Using temperature-dependent properties for air (ideal gas, piecewise polynomials for C_p , kinetic theory for transport properties) enhances the physical realism of the simulation.
- **Boundary Layer Meshing:** The presence of refined layers near the wall (as seen in Figure 4) is good practice for capturing boundary layer effects.
- **Qualitative Capture of Flow Physics:** The simulation qualitatively captured the expected shock structures, pressure/Mach number changes, and turbulence generation patterns for an over-expanded nozzle.

7.2 Areas for Improvement and Further Investigation

- **Shock Resolution:**
 - The shock waves in the contour plots (e.g., Figure 5) appear somewhat smeared or diffused. This is a common issue in CFD and can be attributed to:
 1. **Mesh Coarseness:** The mesh may not be sufficiently fine in the regions where shocks form and interact. Sharper shocks require significantly more grid points across the shock front. Mesh refinement based on pressure or density gradients could be beneficial here.
 2. **Numerical Scheme Order:** While second-order upwind schemes were used, they still possess some numerical dissipation. Higher-order schemes (e.g., third-order MUSCL) or specialized shock-capturing schemes might yield sharper results, but they can be more computationally expensive and sometimes less stable.
 3. **Solver Dissipation:** Some inherent numerical dissipation exists in all solvers.
 - **Impact of Diffuse Shocks:** Diffused shocks can affect the predicted shock location, strength, and the details of shock-boundary layer interaction, which in turn influences potential flow separation and overall nozzle performance metrics.
 - **More Time and Memory:** With a more powerful computer (more memory and CPU cores), a significantly finer mesh could be employed. Running the simulation for more iterations would also allow the solution to converge more accurately to the fine details of the shock system.

8.0 Conclusion

This report has detailed a CFD analysis of an over-expanded, two-dimensional axisymmetric convergent-divergent nozzle using Ansys Fluent with the Transition SST turbulence model. The governing RANS

equations, coupled with the turbulence model and ideal gas law, were solved using a density-based solver with second-order spatial discretization.

The simulation successfully captured some the features of the over-expanded nozzle flow, including:

- Choked flow at the throat and supersonic acceleration in the diverging section.
- The formation of an internal shock system (oblique shocks/Mach reflections) characteristic of over-expansion, leading to recompression of the flow.
- Associated increases in static pressure and temperature, and a significant decrease in total pressure across the shocks.
- Elevated levels of turbulent kinetic energy in the nozzle boundary layers, shock-boundary layer interaction regions, and the shear layers of the exhaust jet.

The choice of the Transition SST model and the solver settings were appropriate for this type of complex, compressible, turbulent flow. The use of temperature-dependent fluid properties added to the physical realism of the simulation.

However, the resolution of the shock structures in the results appears somewhat diffuse, which is likely a consequence of mesh resolution limitations and numerical dissipation. To improve the accuracy and sharpness of the shock capturing, further work involving mesh refinement (potentially adaptive), a rigorous grid independence study, and possibly exploration of higher-order numerical schemes would be beneficial. Quantitative validation against experimental data or benchmark solutions is also an important next step for a complete assessment.

Despite these areas for potential refinement, the current simulation provides insight into the complex flow physics of over-expanded nozzles. It demonstrates the capability of modern CFD tools to predict these challenging flows, highlighting the importance of careful model setup, appropriate turbulence modeling, and adequate mesh resolution, especially in regions with strong gradients such as shock waves. This study reinforces the understanding that computer resources (memory and computational time) are often limiting factors in achieving highly resolved shock structures in practical CFD simulations.

Bibliography

- [1] Anderson, J. D., Jr. (2003). *Modern Compressible Flow: With Historical Perspective* (3rd ed.). McGraw-Hill.
- [2] Sutton, G. P., & Biblarz, O. (2010). *Rocket Propulsion Elements* (8th ed.). John Wiley & Sons.
- [3] Balabel, A., Hegab, A. M., Nasr, M., & El-Behery, S. M. (2011). Assessment of turbulence modeling for gas flow in two-dimensional convergent-divergent rocket nozzle. *Applied Mathematical Modelling*, 35(7), 3408-3422.
- [4] Shapiro, A. H. (1953). *The Dynamics and Thermodynamics of Compressible Fluid Flow* (Vol. 1). Ronald Press.
- [5] Menter, F. R. (1994). Two-equation eddy-viscosity turbulence models for engineering applications. *AIAA Journal*, 32(8), 1598-1605.
- [6] Menter, F. R., Kuntz, M., & Langtry, R. (2003). Ten years of industrial experience with the SST turbulence model. *Turbulence, Heat and Mass Transfer 4*, Begell House, 625-632.
- [7] Menter, F. R., Langtry, R. B., Likki, S. R., Suzen, Y. B., Huang, P. G., & Völker, S. (2009). A correlation-based transition model using local variables—Part I: Model formulation. *Journal of Turbomachinery*, 128(3), 413-422.